Available online at www.sciencedirect.com
ScienceDirect
Journal of Nuclear Materials 375 (2008) 331–339
journal of nuclear materials
www.elsevier.com/locate/jnucmat

Modelling of time resolved and long contact time dissolution studies of spent nuclear fuel in 10 mM carbonate solution – A comparison between two different models and experimental data

Trygve E. Eriksen [a], Mats Jonsson [a,*], Juan Merino [b]

[a] School of Chemical Science and Engineering, Nuclear Chemistry, Royal Institute of Technology, SE-100 44 Stockholm, Sweden
[b] Enviros Spain S.L., Pg. de Rubí, 29-31, E-08197 Valldoreix, Spain

Received 15 November 2007; accepted 18 December 2007

Abstract

Using two different models, radiation induced dissolution of spent UO_2 fuel has been simulated. One of the models is conventional homogeneous radiolysis simulations where two different geometrical constraints were used and the second model is the recently developed steady-state model. The results of the simulations are compared to each other and to experimental results from spent fuel leaching experiments performed in carbonate containing aqueous solution under Ar-atmosphere. The influence of radiolytically produced H_2 is incorporated (on the basis of a recently suggested mechanism) in both models and this reproduces the experimentally observed inhibition of spent fuel dissolution fairly well. The conventional radiolysis model reproduces the experimental concentrations of the radiolysis products H_2 and O_2 very well while it fails to reproduce the experimental H_2O_2 concentration. The reasons for this are discussed. The general trend in uranium concentration as a function of time is reproduced by both the conventional radiolysis model and the steady-state model. The conventional radiolysis model (in which the radiation dose is homogeneously distributed in the whole liquid volume) underestimates the uranium concentration while the steady-state model, which represents the worst case scenario, overestimates the concentrations to some extent. When applying the conventional radiolysis model, assuming that all the radiation energy is deposited within 40 μm from the fuel surface, the uranium concentrations during the initial part of the experiments are reproduced quantitatively. The differences between the models and the applicability of the models are discussed in some detail.

1. Introduction

A key parameter in performance assessment models for permanent disposal of nuclear fuel is the source term for release of radionuclides from the fuel matrix. In the U(IV) state uranium is extremely insoluble and significant release of radionuclides would only be expected in the presence of oxidants able to sustain oxidation of the UO_2-matrix.

Irradiated fuel contains α, β and γ emitting radionuclides and water in contact with the fuel surface will unavoidably be radiolysed by a field of mixed radiation. The water radiolysis produces equivalent amounts of oxidising and reducing radical and molecular species.

In a research programme, started 1995, the mass balance of radiolytically produced oxidants and reductants, (dissolved) released uranium, actinides and fission products has been studied. The experiments were carried out with fragments of irradiated fuel in carbonate and chloride containing solution in closed systems with Ar-gas head space.

The programme encompasses time resolved and long contact time experiments of 10–40 days and 1–3 years duration, respectively.

Experimental data and chemical modelling are presented in several reports [1–4] and publications [5,6].

The data from oxygen and hydrogen analysis of the gas phase and hydrogen peroxide analysis of the aqueous phase

* Corresponding author. Tel.: +46 8 790 9123; fax: +46 8 790 8722.
E-mail address: matsj@nuchem.kth.se (M. Jonsson).

0022-3115/$ - see front matter © 2008 Elsevier B.V. All rights reserved.
doi:10.1016/j.jnucmat.2007.12.003

indicate steady-state conditions for radiolytically formed oxidants and reductants and the concentrations of fission products and actinides were, within the experimental uncertainties, found to be constant within the time interval 400–900 days. The experimental data indicate that the oxidative dissolution of the fuel fragments, although the concentrations of the oxidative radiolysis products (H_2O_2, O_2) remained constant, was suppressed.

Radiolytic modelling of the 10 mM carbonate system encompassing catalytic H_2O_2 decomposition and oxidation of the fuel matrix by H_2O_2 yielded reasonable agreement between calculated and measured concentrations of H_2, O_2 and H_2O_2 for the time resolved experiments but underestimated the initial uranium concentration [4]. Steady-state conditions were not reached in the calculations within the 900 days experimental time period.

A few dissolution and electrochemical experiments have been published demonstrating the suppression of fuel oxidation by H_2 in a radiation field [7–9,25].

Röllin et al. [7] studied the dissolution of spent UO_2 fuel in 10 mM NaCl solution under reducing (H_2), anoxic (Ar) and oxidising (20% O_2, 80% Ar) conditions. Whereas the rates of dissolution in (Ar) and (20% O_2, 80% Ar) saturated solutions were not found to differ significantly the rate of dissolution in the H_2 saturated solutions was found to decrease by up to four orders of magnitude.

King et al. [8] studied the effect of γ-radiation on the corrosion potential E_{corr} of UO_2 in 0.1 M NaCl solution at 5 MPa overpressure of either H_2 or Ar. In the absence of radiation no significant difference was observed in the steady-state E_{corr} of UO_2 measured at Ar or H_2 overpressure. However, in the presence of radiation (11.3–15.9 Gy h^{-1}) H_2 was found to have two effects on the oxidation of UO_2(s). Not only did H_2 suppress the oxidation of UO_2(s) by radiolytic oxidants but it also produced more reducing conditions than observed with H_2 and Ar in the absence of radiation. The rationale for this is most probably the conversion of oxidising hydroxyl radicals into reducing hydrogen atoms.

Broczkowski et al. [9,25] studied electrochemically the effect of H_2 on the corrosion potential in 0.1 M KCl of two 1.5 at.% SIMFUEL electrodes, one with and one without incorporated ε-particles (fission products forming noble metal particles). Using a 5% H_2/95% Ar mixture E_{corr} for the ε-particle containing SIMFUEL was found to be pressure dependent over the total pressure range 0–0.21 MPa. In the absence of ε-particles no substantial change in corrosion potential was observed in solutions saturated with the H_2 containing gas mixture or Ar. The corrosion potential of the electrode with ε-particles was clearly lowered in solution saturated with the H_2 containing gas mixture.

The proposed explanation is a catalytic H_2-dissociation reaction on these particles which act as galvanic anodes within the fuel matrix and reduces oxidised uranium. The net effect would be recombination of H_2O_2 and H_2 to H_2O.

Kinetic studies have shown that the recombination of H_2O_2 and H_2 on noble metal particles is a virtually diffusion controlled process [10]. However, since the surface area covered by noble metal particles is expected to be in the order of 1% or less, this reaction alone would not be able to compete efficiently with the reaction between H_2O_2 and UO_2. Noble metal particles have also been shown to catalyze the reduction of UO_2^{2+} (aq) by H_2 efficiently (diffusion controlled) [11]. Very recent kinetic studies show that this process also occurs in the solid phase [12]. The impact of the latter process on the overall kinetics of spent nuclear fuel dissolution is more substantial and fairly low concentrations of H_2 are expected to be sufficient to completely stop the oxidative dissolution [13]. The processes of oxidative dissolution and noble metal particle catalyzed inhibition by H_2 are summarized in Scheme 1.

In recent years, several papers dealing with the kinetics of the elementary processes involved in oxidative dissolution of UO_2 have been published [14,15]. This type of data opens up new possibilities for modelling of spent nuclear fuel dissolution on the basis of mechanistic and kinetic knowledge rather than empirical relationships.

We here report modelling of experimental data from time resolved and long time experiments with 2–4 mm particles of spent fuel in 10 mM carbonate solution taking into account the effect of carbonate on the dissolution of oxidised fuel and a catalytic reaction between H_2 and ε-particles. Two types of models are employed. The first model is conventional simulation of radiolysis in a homogeneous system and the second model is a simplified steady-state approach which has recently been developed [13,16,17].

2. Experimental

All experiments were carried out in 60 cm^3 glass ampoules containing 2–4 mm diameter fragments of irradiated fuel, 30 cm^3 deoxygenated Ar-saturated 10 mM HCO_3^- solution (pH ≈ 8) with Ar and 30 cm^3 head space (Ar).

The time resolved experiments were carried out with 2 g fragments from PWR-reference fuel Ringhals DO-7-S14 in a glass ampoule fitted to a gas sensor chamber. The gas phase was at time intervals analysed for H_2 and O_2 using Orbisphere detectors. The solution was analysed for H_2O_2 by means of a chemiluminescence method and for

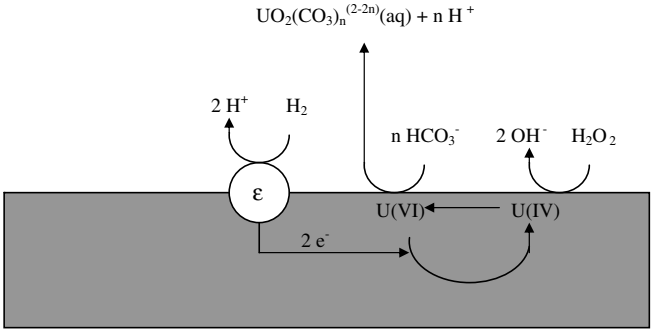

Scheme 1. Elementary processes involved in radiation induced oxidative dissolution of spent nuclear fuel.

actinides and fission products by ICP-MS. The uranium concentration was also measured by laser fluorimetry. Details of the experimental set up and analyses are given in Eriksen et al. [5] and Bruno et al. [2].

The long contact time experiments were carried out with 1 g fragments from Tvålivsstaven 33-25046 in closed ampoules with breakable membranes. At the end of the experiment the ampoule was connected to a gas sampling system and the membrane broken.

The H_2 and O_2 concentrations were measured by mass spectrometry. The solution analyses at the end of the experiments were carried out as in the time resolved experiments.

The time scale was <40 days and 900 days for the time resolved and long contact time experiments, respectively.

3. Modelling

3.1. The steady-state model

On the basis of the kinetics for the elementary processes involved in radiation induced oxidative dissolution of spent nuclear fuel in aqueous solution the relative impact of the different radiolytic oxidants has been assessed [18]. This study shows that, under deep repository conditions, H_2O_2 is by far the most important oxidant in the system. Numerical simulations of the H_2O_2 concentration profile evolution with time in the vicinity of a spent nuclear fuel surface (taking the distance dependent production of H_2O_2, the surface reaction between H_2O_2 and UO_2 and the diffusion of H_2O_2 into account) show that the surface concentration of H_2O_2 fairly rapidly approaches a steady-state value [16,17]. The steady-state concentration corresponds to the system steady-state, i.e. the concentration at which the production of H_2O_2 from radiolysis is balanced by the consumption of H_2O_2 in the surface reaction with UO_2. Consequently, the rate of UO_2 oxidation will rapidly approach a constant value given by the dose rate (i.e. rate of H_2O_2 production). The rate of H_2O_2 consumption on the UO_2 surface is given by the following equation:

$$r_{H_2O_2} = \int_{x=0}^{x_{max}} \dot{D}(x) \times \rho \times G(H_2O_2)\mathrm{d}x, \quad (1)$$

where $\dot{D}(x)$ is the dose rate at distance x from the fuel surface, ρ is the density of water and $G(H_2O_2)$ is the radiation chemical yield for H_2O_2. The dose distribution for spent nuclear fuel is dominated by α- and β-radiation. Furthermore, the oxidation yield for H_2O_2 is approximately 80% (i.e. 80% of the H_2O_2 is consumed by oxidation of UO_2 while the remaining 20% is catalytically decomposed on the UO_2 surface) [19]. Taking these factors into account, the rate of UO_2 (fuel matrix) oxidation can be calculated from the following equation:

$$r_{ox} = 0.8\left(\overline{r_{H_2O_2}(\alpha)}\delta_{max}(\alpha) + \overline{r_{H_2O_2}(\beta)}\delta_{max}(\beta)\right), \quad (2)$$

where $\bar{r}$ is the average H_2O_2 production rate (Eq. (1)) and δ is the maximum range of the radiation.

Comparison to experimental data on spent nuclear fuel dissolution shows that the steady-state model gives surprisingly good agreement with the experimental data [20].

The combined effect of H_2 and ε-particles can also be accounted for in the steady-state model. In general, the ε-particle catalyzed reduction of oxidised UO_2 on the fuel surface competes with dissolution of the oxidised UO_2 (Scheme 1). In a system where the HCO_3^- concentration is higher than 1 mM, the rate limiting step is oxidation of UO_2. Consequently, the rate of dissolution can be described by the following equation:

$$r_{diss} = r_{ox} - k_{H_2}[H_2]\varepsilon_{rel}, \quad (3)$$

where r_{diss} is the dissolution rate, r_{ox} is the oxidation rate, k_{H_2} is the rate constant for the reaction between H_2 and the ε-particles, $[H_2]$ is the concentration of H_2 and ε_{rel} is the fraction of the fuel surface area covered by ε-particles.

3.2. Conventional simulation of radiolysis in a homogeneous system

3.2.1. Dose rates

The α and β dose rate distributions in solution are calculated for both sets of experiments, based on the fuel inventories as given by OrigenArp 2.00 calculations carried out at Hot Cell Laboratory, Studsvik AB. Details of the method used are given in Cera et al. [4].

In the radiolysis calculation we have chosen to treat the bulk volume of solution as irradiated, i.e. to average the α and β doses within the total volume. The γ-radiation is neglected in the calculations.

3.3. Radiation chemical yields

The radiation chemical yields of primary species used in the modelling are given in Table 1.

3.4. Radiation induced reactions

The calculations are carried out using the computer code Maksima Chemist [21] and the radiolytic reaction scheme (reactions 1–55) given in Table 2a.

The surface reactions (56–59) are, due to the limitations of the computer code, written as homogeneous reactions.

Table 1
Primary yields of products (mol J^{-1}) × 10^7 formed upon radiolysis of water

Species	β	α
H_2O	−4.30	−2.87
H_2	0.45	1.30
H_2O_2	0.75	0.985
e^-_{aq}	2.8	0.06
H	0.6	0.21
OH	2.8	0.24
H^+	2.8	0.06
HO_2	–	0.22

Table 2a
Radiolytic reaction scheme

No.	Reactants	Products	Rate constant ($M^{-1} s^{-1}$)
1	$OH^{\cdot} + OH^{\cdot}$	H_2O_2	5.500×10^9
2	$OH^{\cdot} + e^-_{aq}$	OH^-	3.000×10^{10}
3	$OH^{\cdot} + H^{\cdot}$	H_2O	7.000×10^9
4	$OH^{\cdot} + O_2^{\cdot-}$	$OH^- + O_2$	1.000×10^{10}
5	$OH^{\cdot} + HO_2^{\cdot}$	$O_2 + H_2O$	6.000×10^9
6	$OH^{\cdot} + H_2O_2$	$H_2O + O_2^{\cdot-} + H^+$	2.700×10^7
7	$OH^{\cdot} + H_2$	$H_2O + H$	4.000×10^7
8	$OH^{\cdot} + HO_2^-$	$HO_2 + OH^-$	7.500×10^9
9	$e^-_{aq} + e^-_{aq}$	$OH^- + OH^- + H_2$	5.500×10^9
10	$e^-_{aq} + H^{\cdot}$	$OH^- + H_2$	2.000×10^{10}
11	$e^-_{aq} + HO_2^{\cdot}$	HO_2^-	2.000×10^{10}
12	$e^-_{aq} + O_2^{\cdot-}$	$HO_2^- + OH^-$	1.200×10^{10}
13	$e^-_{aq} + H_2O_2$	$OH + OH^-$	1.600×10^{10}
14	$e^-_{aq} + H^+$	H	2.200×10^{10}
15	$e^-_{aq} + O_2$	$O_2^{\cdot-}$	1.200×10^{10}
16	$e^-_{aq} + H_2O$	$H^{\cdot} + OH^-$	2.000×10^1
17	$H^{\cdot} + H^{\cdot}$	H_2	1.000×10^{10}
18	$H^{\cdot} + HO_2^{\cdot}$	H_2O_2	2.000×10^{10}
19	$H^{\cdot} + O_2^{\cdot-}$	HO_2^-	2.000×10^{10}
20	$H^{\cdot} + H_2O_2$	$OH^{\cdot} + H_2O$	6.000×10^7
21	$H^{\cdot} + OH^-$	$e^-_{aq} + H_2O$	2.000×10^7
22	$H^{\cdot} + O_2$	$O_2^{\cdot-} + H^+$	2.000×10^{10}
23	$HO_2^{\cdot}$	$O_2^{\cdot-} + H^+$	8.000×10^5
24	$HO_2^{\cdot} + HO_2^{\cdot}$	$O_2 + H_2O_2$	7.500×10^5
25	$HO_2^{\cdot} + O_2^{\cdot-}$	$O_2 + HO_2^-$	8.500×10^7
26	$O_2^{\cdot-} + H^+$	$HO_2^{\cdot}$	5.000×10^{10}
27	$H_2O_2 + OH^-$	$HO_2^- + H_2O$	5.000×10^8
28	$HO_2^- + H_2O$	$H_2O_2 + OH^-$	5.735×10^4
29	H_2O	$H^+ + OH^-$	2.599×10^{-5}
30	$H^+ + OH^-$	H_2O	1.430×10^{11}
31	$CO_2 + H_2O$	$HCO_3^- + H^+$	2.000×10^4
32	$HCO_3^- + H^+$	$CO_2 + H_2O$	5.000×10^{10}
33	HCO_3^-	$CO_3^{2-} + H^+$	2.000
34	$CO_3^{2-} + H^+$	HCO_3^-	5.000×10^{10}
35	$CO_2 + e^-_{aq}$	$CO_2^{\cdot-}$	7.700×10^9
36	$CO_3^{2-} + e^-_{aq}$	$CO_2^{\cdot-} + OH^- + OH^-$	3.900×10^5
37	$HCO_3^- + H^{\cdot}$	$CO_3^{\cdot-} + H_2$	4.400×10^4
38	$OH^{\cdot} + HCO_3^-$	$CO_3^{\cdot-} + H_2O$	8.500×10^6
39	$OH^{\cdot} + CO_3^{2-}$	$CO_3^{\cdot-} + OH^-$	3.900×10^8
40	$CO_3^{\cdot-} + CO_3^{\cdot-}$	$CO_4^{2-} + CO_2$	7.000×10^6
41	$CO_4^{2-} + H_2O$	$CO_2 + HO_2^- + OH^-$	2.000×10^{-1}
42	$CO_3^{\cdot-} + H_2O_2$	$CO_3^{2-} + HO_2^{\cdot} + H^+$	8.000×10^5
43	$CO_3^{\cdot-} + HO_2^-$	$CO_3^{2-} + O_2^{\cdot-} + H^+$	1.000×10^7
44	$CO_3^{\cdot-} + O_2^{\cdot-}$	$CO_3^{2-} + O_2$	6.005×10^8
45	$CO_3^{\cdot-} + CO_2^{\cdot-}$	$CO_3^{2-} + CO_2$	3.000×10^8
46	$CO_2^{\cdot-} + e^-_{aq}$	$HCOO^- + OH^-$	9.000×10^8
47	$CO_2^{\cdot-} + CO_2^{\cdot-}$	$C_2O_4^{2-}$	5.000×10^8
48	$CO_2^{\cdot-} + H_2O_2$	$CO_2 + OH^{\cdot} + OH^-$	6.000×10^5
49	$CO_2^{\cdot-} + O_2$	$CO_2 + O_2^{\cdot-}$	2.000×10^9
50	$CO_2^{\cdot-} + HCO_3^-$	$CO_3^{\cdot-} + HCOO^-$	2.000×10^3
51	$CO_3^{\cdot-} + HCOO^-$	$HCO_3^- + CO_2^{\cdot-}$	1.500×10^5
52	$OH^{\cdot} + HCOO^-$	$CO_2^{\cdot-} + H_2O$	3.200×10^9
53	$H^{\cdot} + HCOO^-$	$CO_2^{\cdot-} + H_2$	2.100×10^8
54	$e^-_{aq} + HCOO^-$	$CO_2^{\cdot-} - H^+ + H_2$	8.000×10^8
55	$OH^{\cdot} + C_2O_4^{2-}$	$CO_2^{\cdot-} + CO_2 + OH^-$	4.000×10^7

The conversion is achieved by assuming that the number of sites in a monomolecular layer on the surface is dissolved in the solution volume. The site density is taken to be 2.74×10^{-4} mol m^{-2} [22]. The rate constants are calculated from 7.3×10^{-8} m s^{-1} [15] for the reaction between $>UO_2$ and $H_2O_2$and assuming the reaction between H_2 and ε-particles to be diffusion controlled ($\sim 10^{-6}$ m s^{-1}). The corresponding converted rate constants used in the assumed homogeneous system are 0.27 and 3.7 $M^{-1} s^{-1}$, respectively. The surface reactions are summarized in Table 2b. It should be pointed out that the site density used in the conversion does not influence the simulations since both the available surface area and the rate constants are converted using this number (when combined in the rate expression they cancel each other).

Table 2b
Surface reactions

No.	Reactants	Products	Rate constant ($M^{-1} s^{-1}$)
56	$H_2O_2 + >UO_2$	UO_2^{2+}(surf) + $2OH^-$	2.700×10^{-1}
57	UO_2^{2+}(surf) + HCO_3^-	UO_2CO_3 (aq) + H^+	Varied
58	$H_2 + \varepsilon$	$\varepsilon - 2e^- + 2H^+$	3.700
59	UO_2^{2+}(surf) + $\varepsilon - 2e^-$	$>UO_2 + \varepsilon$	Fast

Table 2c
Gas/solution distribution of the radiolysis products O_2 and H_2

No.	Reactants	Products	Rate constant ($M^{-1} s^{-1}$)
60	O_2(sol)	O_2(gas)	1.000×10^{-3}
61	H_2(sol)	H_2(gas)	1.000×10^{-3}
62	O_2(gas)	O_2(sol)	3.137×10^{-5}
63	H_2(gas)	H_2(sol)	1.900×10^{-5}

Whereas the rate constant for carbonate complexation with UO_2^{2+}(surf) according to Merino et al. [23], based on experimental data by de Pablo and coworkers, is 5.00×10^{-2} $M^{-1} s^{-1}$. Hossain et al. [15] have found the reaction to be diffusion controlled, i.e. $k(57) \approx 3.7$ $M^{-1} s^{-1}$. The latter rate constant 3.7 was used in the calculations, with the exception for data shown in Fig. 5.

The gas/solution distribution of the radiolysis products O_2 and H_2 are given by reactions 60–63 in Table 2c.

The ratio between the back reaction rates $k(62,63)$ and the forward reaction rates $k(60,61)$ is given by the following equation:

$$\frac{k_b}{k_f} = \frac{V_{sol}}{V_{sol} + \frac{V_{gas}}{22.4 K_s}} \quad (4)$$

The solubility in water, K_s, is 0.85 and 1.4 mM for H_2 and O_2, respectively [24].

4. Results and discussion

The concentrations of radiolytically produced H_2 and O_2 in the time resolved and long contact time experiments as a function of time are shown in Figs. 1 and 2, respectively. The corresponding data obtained from radiolytic simulations, taking 1% noble metal particle surface coverage into account, are also included in the plots. The two simulation lines describe the time resolved and long contact time experiments, respectively. The experimental condi-

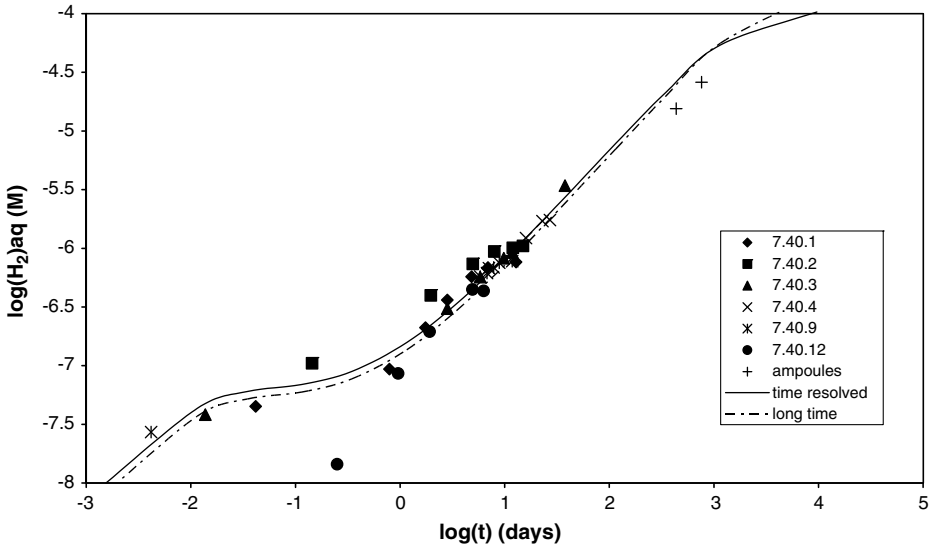

Fig. 1. Experimental and calculated hydrogen concentrations in solution plotted as function of time. Radiolysis simulations including surface reactions with 1% surface coverage of noble metal particles.

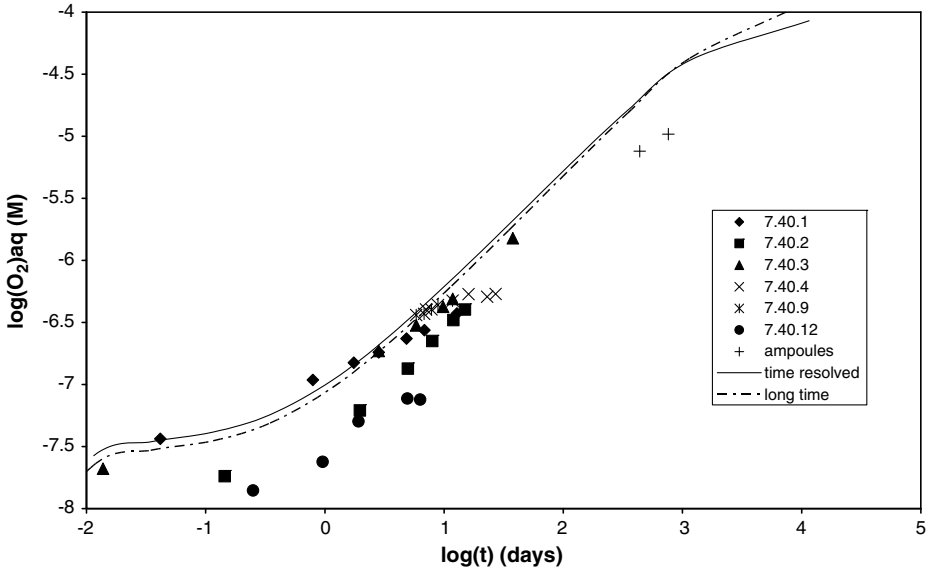

Fig. 2. Experimental and calculated oxygen concentrations in solution plotted as function of time. Radiolysis simulations including surface reactions with 1% surface coverage of noble metal particles.

tions (dose rate and amount of fuel) are slightly different for the two sets of experiments.

As can be seen the calculated H_2 concentration–time plot is in good agreement with the experimental data. The calculated O_2 concentration–time plot displays somewhat higher concentrations than the experimentally measured ones over the whole time period studied.

The H_2O_2 and U concentrations from the same experiments are plotted versus time in Figs. 3 and 4, respectively. The uranium concentrations are corrected for sample volumes removed for analysis.

Experiment 7.40.1 was the first with the fuel fragments used in the time resolved series and instant uranium release from a partially preoxidised fuel surface was observed.

The radiolytic simulations clearly give too high H_2O_2 concentration and initially too low U concentration in the solution. For comparison, the experimental U concentrations after one day and for the long term experiments are given in Table 3 along with the corresponding values obtained in the simulations.

The rate of UO_2 oxidation by H_2O_2 is underestimated in the calculations which will render slightly too high O_2concentrations in the solution as O_2 production becomes the major pathway for H_2O_2 consumption.

These differences can be explained by the dose distributions for α- and β-radiation in the solution. Whereas the range of β is 3–5 mm in water the α-energy is absorbed within 40 μm from the fuel surface and the dose rate and

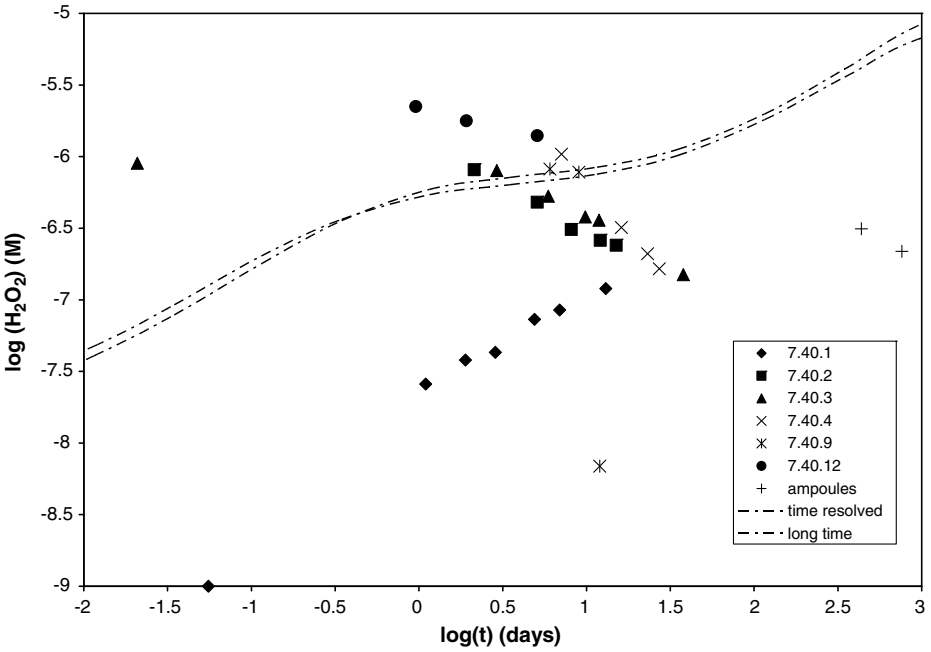

Fig. 3. Experimental and calculated hydrogen peroxide concentrations in solution plotted as function of time. Radiolysis simulations including surface reactions with 1% surface coverage of noble metal particles.

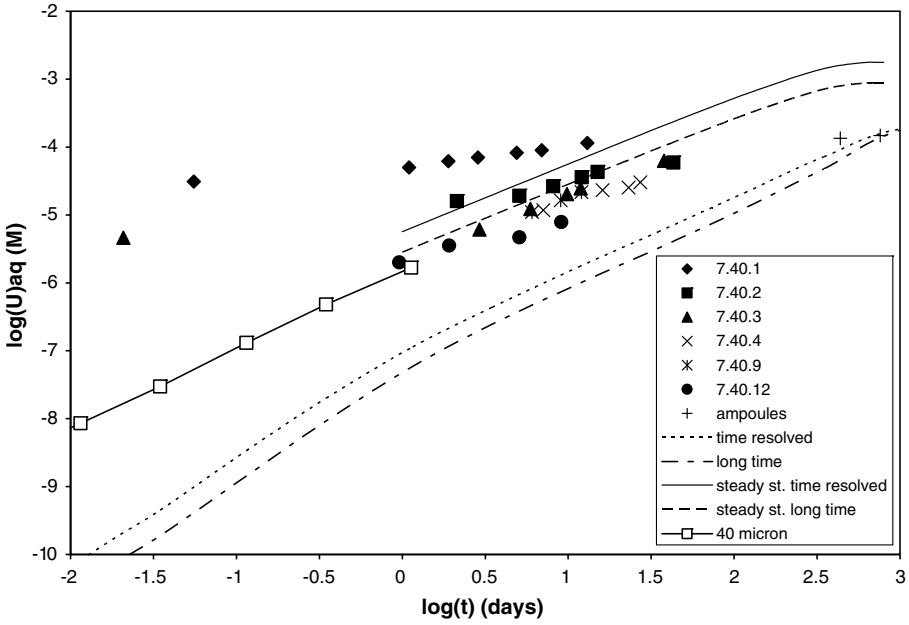

Fig. 4. Experimental and calculated uranium concentrations in bulk solution plotted as function of time. Modelling based on average dose rates in bulk solution, 40 μm layer of solution in contact with the fuel surface and steady-state hydrogen peroxide concentration, respectively.

radiolytic yields of the primary molecular products H_2 and H_2O_2 close to the particle surface are much higher than the volume averaged molecular yields and dose rates used in the simulations.

Using the α and β dose rates within 40 μm distance from the particle surface, the radiation field averaged G-values, the reaction scheme given in Table 1 and taking into account the diffusion of molecular species out of the α–β irradiated volume we have calculated the initial rate of oxidation of the UO_2-surface by H_2O_2.

The diffusion is estimated using the following equation:

$$\frac{dC}{dt} = \frac{A \times D}{V} \times \frac{dC}{dx}, \tag{5}$$

Table 3
Measured and calculated uranium concentrations (M) in 30 cm^{-3} bulk solution

Time (days)	Uranium concentration (M)					
	Exp.	Radiolysis model		Steady-state model		40 μm water layer
		TR	LT	TR	LT	TR
1	$(2 \pm 1.3) \times 10^{-6}$	1.12×10^{-7}	3.98×10^{-8}	5.65×10^{-6}	2.83×10^{-6}	1.47×10^{-6}
398	1.34×10^{-4}	8.0×10^{-5}	5.25×10^{-5}	1.54×10^{-3}	7.68×10^{-4}	
759	1.48×10^{-4}	1.42×10^{-4}	1.1×10^{-4}	1.76×10^{-3}	8.82×10^{-4}	

Modelling based on radiolysis, steady-state (H_2O_2) concentration and 40 μm innermost water layer approach.
TR, time resolved; LT, long contact time.

where C is the concentration; D is the diffusion constant; A is the spent fuel particle surface area; V is the irradiated volume; x is the thickness of the irradiated water layer.

The initial rate of UO_2 release taking the dose distribution in close proximity to the fuel surface into account is also included in Fig. 4.

As can be seen the calculated initial rate of oxidation ties well in with the experimental data clearly demonstrating the importance of the H_2O_2 concentration in the innermost water layer.

In the work underlying the steady-state approach, the H_2O_2 concentration profile as a function of time was simulated [16,17]. The resulting profiles clearly show that diffusion out of the irradiated volume rapidly becomes of minor importance. When averaging the dose in the whole volume in the conventional radiolysis calculations, diffusion is in practice highly overestimated as all the radiolysis products instantly become homogeneously distributed in the system. In this case, the H_2O_2 concentration at the surface is underestimated.

Uranium concentrations in solution calculated using the steady-state approach, taking 1% noble metal particle surface coverage into account, for the time resolved and long contact time experiments are also plotted in Fig. 4. The calculated concentrations are somewhat too high but follow nicely the time dependence of the experimental data. As pointed out above, the steady-state approach gives the maximum dissolution rate. The steady-state surface concentration of H_2O_2 is assumed to be reached instantly in the simulation. In reality, however, some time is required before surface steady-state is reached. The initial increase in uranium concentration is therefore somewhat lower than expected from the simulation. For longer times, the rate of dissolution obtained from the simulation is in good agreement with the experimental results.

The relative importance of radicals in radiation induced oxidative dissolution of spent nuclear fuel has been discussed for several decades. In the recent study mentioned above, the relative importance of oxidative radiolysis products was assessed. The results clearly showed that radicals such as $OH^{\bullet}$ and $CO_3^{\bullet-}$ are of minor importance [19]. In the two models used in this work, the only oxidant accounted for in the process of UO_2 oxidation is H_2O_2. The assessment is indeed supported by the good agreement between the model results and experimental results both in terms of absolute uranium concentrations and rate of dissolution. Numerical simulations of homogeneous radiation chemistry in aqueous solution also show that radical–radical reactions involving short-lived radicals are of no importance for the overall water chemistry under deep repository conditions. The reason for this is that the radical concentrations are very low at the dose rates and radiation chemical yields (G-values) of relevance. This also explains why the radiolytical simulation, where the dose is averaged over the whole liquid volume, reproduces the H_2 and O_2 concentrations quite accurately. This would not be the case if radical–radical reactions were of significance, as the total amount of the radiolysis products would depend on the actual volume in which the radiation energy is deposited. Consequently, radical–radical reactions for short-lived radicals can be omitted when simulating radiation chemistry for a deep repository.

The large discrepancy between the reported values for HCO_3^- facilitated dissolution of UO_2^{2+} is a potential problem. However, when a system containing high concentrations of HCO_3^- has reached steady-state this discrepancy will be of minor importance for a system. The simulations show that the overall behaviour is not affected by the rate constant of this reaction. The main rationale for this is that the surface coverage of UO_2^{2+} is extremely low (Fig. 5).

As can be seen in Fig. 5, the time after which the H_2 inhibition mechanism becomes faster than the HCO_3^- facilitated dissolution of UO_2^{2+} is virtually the same for both rate constants.

When included in the simulations, the noble metal particle catalyzed H_2 inhibition mechanism and the rate constants determined from simple model systems fully account for the experimentally observed results, i.e. the initial rate of dissolution and the fact that the process is completely inhibited after approximately 500 days. Consequently, the mechanism outlined in Scheme 1 appears to be sufficient to describe radiation induced dissolution of spent nuclear fuel under the conditions used in the present experiments. The magnitude of the H_2-effect under the expected deep repository conditions (i.e. higher H_2 concentrations due to anoxic corrosion of iron) has recently been published [13].

Both methods used in this paper reproduce the experimental results fairly accurately. The steady-state approach

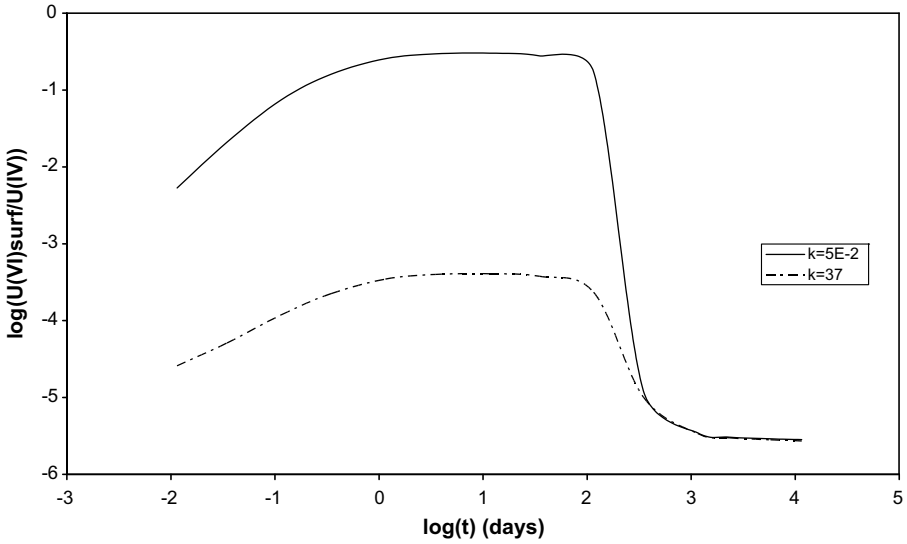

Fig. 5. Effect of rate constant for HCO_3^- facilitated dissolution of oxidised fuel surface (reaction 57) on the concentration of UO_2^{2+} (surf).

has the advantage of being very simple and can be used for fast and sufficiently accurate simulations. To improve the quality of the simulations methods fully accounting for the system heterogeneity must be used. Considering the complexity of the systems of relevance, such simulations would probably not improve the quality and reliability of the safety analysis significantly.

5. Conclusions

The two methods used in this work (conventional radiolysis modelling and the steady-state approach) reproduce the experimental uranium dissolution data fairly accurately when the noble metal particle catalyzed H_2 reduction process is incorporated. The conventional radiolysis model underestimates the uranium concentrations while the steady-state approach overestimates the uranium concentrations. The difference in the results is attributed to completely different treatment of H_2O_2 diffusion.

Conventional radiolysis modelling also reproduces the concentrations of the molecular radiolysis products H_2 and O_2 with high accuracy. The good agreement between the simulations and the spent nuclear fuel leaching data supports the previously suggested mechanism for H_2 inhibition and the previously found low impact of short-lived radicals on the process of spent nuclear fuel dissolution.

Acknowledgement

SKB is gratefully acknowledged for financial support.

References

[1] J. Bruno, E. Cera, L. Duro, J. Pon, J. de Pablo, T.E. Eriksen, Development of a kinetic model for the dissolution of UO_2 spent fuel, Application of the model to minor nuclides, SKB Technical Report 98-22, 1998.
[2] J. Bruno, E. Cera, M. Grivé, U.-B. Eklund, T.E. Eriksen, Experimental determination and chemical modelling of radiolytic processes at the spent fuel/water interface, SKB Technical Report TR-99-26, 1999.
[3] J. Bruno, E. Cera, M. Grive', L. Duro, T.E. Eriksen, Experimental determination and chemical modelling of radiolytic processes at the spent fuel/water interface, Experiments carried out in carbonate solutions in the absence and presence of chloride, SKB Technical Report TR-03-03, 2003.
[4] E. Cera, J. Bruno, L. Duro, T. E. Eriksen, Experimental determination and chemical modelling of radiolytic processes at the spent fuel/water interface, Long contact time experiments, SKB Technical Report TR-06-07, 2006.
[5] T.E. Eriksen, U.-B. Eklund, L. Werme, J. Bruno, J. Nucl. Mater. 227 (1995) 76.
[6] J. Bruno, E. Cera, L. Duro, T.E. Eriksen, L. Werme, J. Nucl. Mater. 238 (1996) 110.
[7] S. R öllin, K. Spahiu, U.-B. Eklund, J. Nucl. Mater. 297 (2001) 231.
[8] F. King, M.J. Quinn, N.H. Miller, The effect of hydrogen and γ radiation on the oxidation of UO_2 in 0.1 mol dm^{-3} NaCl solution, SKB Technical Report TR-99-27, 1999.
[9] M.E. Broczkowski, J.J. Noel, D.W. Shoesmith, J. Nucl. Mater. 346 (2005) 16.
[10] S. Nilson, M. Jonsson, J. Nucl. Mater. 372 (2008) 160.
[11] S. Nilsson, M. Jonsson, J. Nucl. Mater. 374 (2008) 290.
[12] M. Trummer, S. Nilsson, M. Jonsson, J. Nucl. Mater., submitted for publication.
[13] M. Jonsson, F. Nielsen, O. Roth, E. Ekeroth, S. Nilsson, M.M. Hossain, Environ. Sci. Technol. 41 (2007) 7087.
[14] E. Ekeroth, M. Jonsson, J. Nucl. Mater. 322 (2003) 242.
[15] M.M. Hossain, E. Ekeroth, M. Jonsson, J. Nucl. Mater. 358 (2006) 202.
[16] F. Nielsen, K. Lundahl, M. Jonsson, J. Nucl. Mater. 372 (2008) 32.
[17] F. Nielsen, M. Jonsson, J. Nucl. Mater. 374 (2008) 281.
[18] E. Ekeroth, O. Roth, M. Jonsson, J. Nucl. Mater. 355 (2006) 38.
[19] M. Jonsson, E. Ekeroth, O. Roth, Mater. Res. Soc. Symp. Proc. 807 (2004) 77.
[20] F. Nielsen, E. Ekeroth, T.E. Eriksen, M. Jonsson, J. Nucl. Mater. 374 (2008) 286.

[21] M.B. Carver, D.V. Hanley, K.R. Chaplin, Maksima-Chemist. A Program for Mass Action Kinetics Simulation by Automatic Chemical Equation and Integration Using Stiff Techniques, Chalk River Nuclear Laboratories, Chalk River, Ontario, 1979.
[22] F. Clarens, J. de Pablo, I. Casas, J. Giménez, M. Rovira, Mater. Res. Soc. Symp. Proc. 807 (2004) 71.
[23] J. Merino, E. Cera, J. Bruno, J. Quinones, I. casas, F. Clarens, J. Gime'nez, J. de Pablo, M. Roviera, A. Martinez-Esparza, J. Nucl. Mater. 346 (2005) 40.
[24] CRC Handbook of Chemistry and Physics, 46th Ed., 1965.
[25] J.C. Wren, D.W. Shoesmith, S. Sunder, J. Electrochem. Soc. 152 (11) (2005) 470.